energies

Article

Research on Thermal Adaptability of Flexible Operation in Different Types of Coal-Fired Power Units

Haijiao Wei [1], Yuanwei Lu [2,*], Yanchun Yang [3], Yuting Wu [2], Kaifeng Zheng [1] and Liang Li [4]

1 China North Vehicle Research Institute, Beijing 100072, China; weihaijiao1@126.com (H.W.); zhengkaifeng1111@163.com (K.Z.)
2 Key Laboratory of Enhanced Heat Transfer and Energy Conservation, Faculty of Mechanical and Energy Engineering, Beijing University of Technology, Beijing 100124, China; wuyuting@bjut.edu.cn
3 School of Energy and Power Engineering, Inner Mongolia University of Technology, Hohhot 010051, China; 18340313518@163.com
4 Inner Mongolia Daihai Power Generation Co., Ltd., Liangcheng County, Ulanqab 013750, China; jwenku@126.com
* Correspondence: luyuanwei@bjut.edu.cn

Abstract: The flexible mode of operation of coal-fired units can accommodate large-scale renewable power integration into the grid, providing more grid capacity. The flexibility transformation of coal-fired units in thermal power plants can be achieved through main steam extraction and reheated steam extraction. A 300 MW subcritical unit, 600 MW subcritical unit and 660 MW ultra-supercritical unit with six flexible operation modes were chosen as the research model to investigate the thermal adaptability for flexible operation. The results show that from the perspective of the source of steam extraction, the main steam extraction scheme is suitable for the flexible adjustment of peak load capacity, and the reheated extraction scheme is suitable for the flexible operation of low load and high thermal efficiency. Moreover, from the perspective of thermal performance adaptability, the 600 MW unit has a wider load regulation capacity than the 300 MW and 660 MW units, and is suitable as the peak shaving unit. This work can provide theoretical guidance for different types of coal-fired units in choosing flexible operation schemes.

Keywords: coal-fired power unit; main steam extraction; reheated steam extraction; thermal energy storage; flexible operation

Citation: Wei, H.; Lu, Y.; Yang, Y.; Wu, Y.; Zheng, K.; Li, L. Research on Thermal Adaptability of Flexible Operation in Different Types of Coal-Fired Power Units. *Energies* **2024**, *17*, 2185. https://doi.org/10.3390/en17092185

Academic Editor: Ahmed Abu-Siada

Received: 5 April 2024
Revised: 29 April 2024
Accepted: 30 April 2024
Published: 2 May 2024

1. Introduction

Both the energy crisis and sustainability of energy have been considered the main factors restricting human development [1,2]. Additionally, the utilization of clean energy is an inevitable choice. The energy consumption mode will gradually develop to include clean and low-carbon renewable energy [3,4]. However, both the unpredictability [5] and discontinuity [6] of renewable energy can result in unstable power, which can seriously affect the power quality and the safety of the grid [7].

In order to improve the stability of renewable energy power generation entering the grid, scholars have proposed the integration of energy storage devices (e.g., gravity energy storage [8], thermal energy storage [9] and pumped hydropower storage [10]) with the renewable energy system to achieve a stable power output. However, with an increased installed capacity of renewable energy, the space provided by the grid for large-scale renewable energy is limited. So, improving the flexible operation of the coal-fired power unit (CFPU) [11,12] could increase the proportion of renewable energy access to the grid.

The existing literature shows that the flexible operation of CFPU can be achieved by using steam extraction and thermal energy storage [13]. Wei et al. [14] selected a 600 MW subcritical CFPU as an example to analyze the peak shaving capability, which found that the load of the unit decreased from 50%THA to 35%THA by steam extraction and thermal energy storage. Cao et al. [15] proposed the use of reheated steam extraction and thermal energy storage for 660 MW CFPU, along with the use of the stored heat to heat the feedwater in order to generate steam to drive the pump, thereby expanding the operating range of the CFPU from 198–660 MW to 188.41–685.15 MW. There are other [16–18] studies like the ones mentioned above, which will not be introduced in detail here. In addition to steam extraction and thermal energy storage, electric heat storage is also a means to achieve the deep peak shaving of CFPU. Cao et al. [19,20] utilized excess electric power to heat the molten salt. The power output of the 600 MW subcritical unit can be decreased to 500 MW from 600 MW, which increased the peak shaving capacity of 16.67% rated power. The unit load was increased to 106% rated power during the discharging process. These studies provide guiding principles for the integration of deep peak shaving.

In addition to studying the system integration method of CFPU, additional research has also been conducted on system parameters and integration modes related to heat storage and release. Wei et al. [13] studied the influence of the main steam extraction parameters and the unit load of the 600 MW subcritical CFPU on the flexible operation. Wei et al. [21] also studied the super/reheated steam integrated with 600 MW CFPU for flexible operation, considering that the efficiency of reheated steam extraction for thermal energy storage is higher. Wang et al. [22] proposed four deep peak shaving modes. Moreover, the maximum deep peak shaving capability was achieved through the method of extracted super steam and thermal energy storage. Ma et al. [23] have designed eight peak shaving schemes. One conclusion is the coupling of the intermediate-pressure steam turbine exhaust and electric heating molten salt; it was discovered that the molten salt heating bypassed water is the best deep peak shaving mode. These studies provide theoretical support for the integration of deep peak shaving.

The research mentioned above has achieved the flexible operation of CFPU with thermal energy storage schemes, and the unit load has been further reduced. The scheme integration method, parameter analysis and integration modes of the abovementioned studies were analyzed. However, the steam turbine extraction can cause many changes in operating conditions. These include the steam flow rate at the inlet of the low-pressure steam turbine being lower than the safe steam flow rate (30% rated steam flow rate) [24], which will cause the last-stage blade of the turbine to perform negatively. The lower steam flow rate into the low-pressure steam turbine results in steam excited vibration [25] or blade flutter [12]. In addition, as the extraction flow rate of the turbine system increases, the steam pressure at each stage of the extraction port decreases. When the saturated temperature corresponding to the pressure at the extracted steam port of the last stage is the same as the drainage temperature, the last regenerative heat exchanger needs to be cut off. The operation mode of the original unit will be changed.

Facing the above mentioned issues and the impact of different extraction methods on different types of CFPU, a new analysis for thermal adaptability of deep peak shaving is proposed. Therefore, this paper investigates the thermal adaptability in different types of CFPU when utilizing the flexible operation scheme of the main steam and reheated steam extraction. This research has not been reported; furthermore, the basis concerning the selection of the flexible operation scheme of CFPU is acknowledged.

This paper not only clarifies the coupling and synergistic mechanism among the thermal parameters of the unit, the extracted steam parameters and the flexible operation load by using main steam and reheated steam extraction, but also achieves thermal adaptability in different unit types for different working scenarios. The main research objectives of this paper are to establish the flexible operation model of CFPU with the main steam and reheated steam extraction, investigate the steam extraction parameters effect on the load-reduction capacity of the unit, achieve the lower and upper limits of flexible operation load, obtain the peak shaving time and realize the thermal adaptability of different schemes to the CFPU.

2. Studied System

In this paper, the 300 MW unit, 600 MW unit and 660 MW unit are selected to establish the flexible operation model with the main steam extraction and reheated steam extraction, as shown in Table 1. The 300 MW and 600 MW units are the subcritical CFPUs. The 660 MW unit is the ultra-supercritical CFPU.

Table 1. Unit type.

Unit Level	Rated Power (MW)	Type
300 MW unit	300.19	Subcritical, single reheat, direct air-cooled unit
600 MW unit	600.18	Subcritical, single reheat, direct air-cooled unit
660 MW unit	660.02	Ultra-supercritical, single reheat, direct air-cooled unit

The system stores the sensible heat through the molten salt, while the latent heat of the main steam is stored in the phase-change material (the phase-change temperature is determined by the steam pressure). Pressure water is used to store latent heat when the pressure of reheated steam is low.

2.1. CFPU Integrating with the Main Steam Extraction

Figure 1 shows the flexible operation system of CFPU, which includes the traditional CFPU, charging system and discharging system. In the thermal system of the traditional CFPU, the main steam generated by the boiler passes through the high-pressure steam turbine (HP), the re-heater, the intermediate-pressure steam turbine (IP) and the low-pressure steam turbine (LP) to complete the power-generation process. The condensate water (low-pressure exhaust enters the condenser and condenses into water, and the pressure water at the outlet of the condensate pump is called condensate water) is pumped into the eighth reheater (RH8). The pressure water at the outlet of the feedwater pump is called feedwater, which is pumped from RH4 to RH3 by the feedwater pump (FP). In addition, RH1–RH8 extract steam from the turbine. The drainage water is gradually drained from RH1 to RH4. In particular, RH8 is only set in the 660 MW unit. The 660 MW unit has eight regenerative heaters, and the 300 MW and 600 MW units have seven regenerative heaters, respectively.

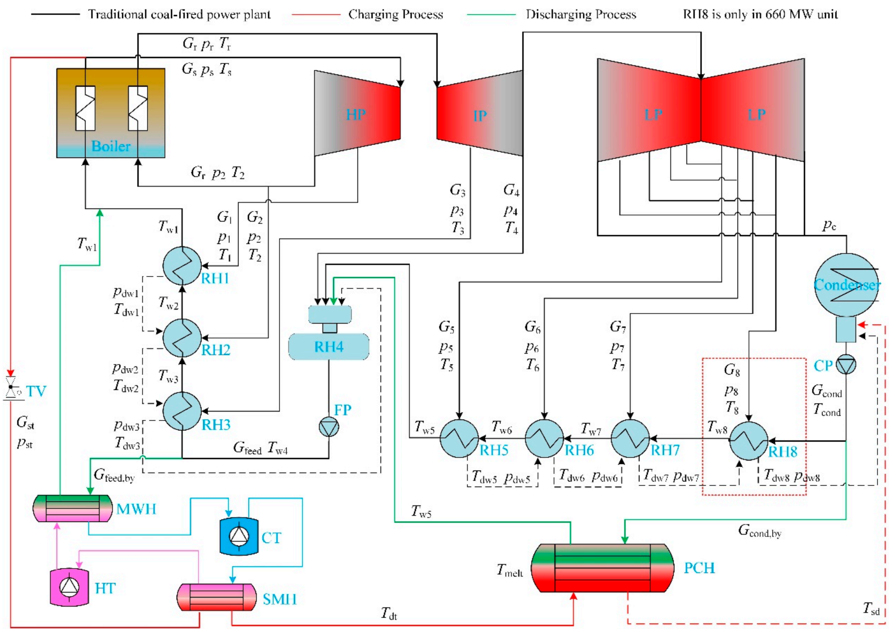

Figure 1. Flexible operation system of CFPU with main steam extraction and thermal energy storage.

The traditional CFPU and the charging system operate simultaneously in the load-reduction process. The main steam enters the steam–molten salt heat exchanger (SMH) through equal enthalpy pressure reduction in the throttle valve (TV). The phase-change material is heated by cooling the extracted main steam and entering the phase-change heat exchanger (PCH) for heating. The condensate pressured water flows back to RH4. Thus, the unit achieves the load-reduction operation.

The traditional CFPU and the discharging system operate simultaneously in the load-raising process. Part of the condensate water at the outlet of the condensate pump enters RH8–RH4, successively. The other part condensate water enters RH4 with the same parameters at the outlet of RH5 after being heated by the PCH. The feed water at the outlet of the feed water pump flows into RH3–RH1 and the boiler. The heated feed water enters the boiler with same parameters at the outlet of RH1. The cooled molten salt returns to the CT. Thus, the unit realizes the load-raising operation.

2.2. CFPU Integrating with the Reheated Steam Extraction

Figure 2 shows the system of CFPU with the reheated steam extraction and thermal energy storage, which also includes the traditional CFPU, charging system and discharging system. The thermodynamic model of the traditional CFPU is described in Figure 1.

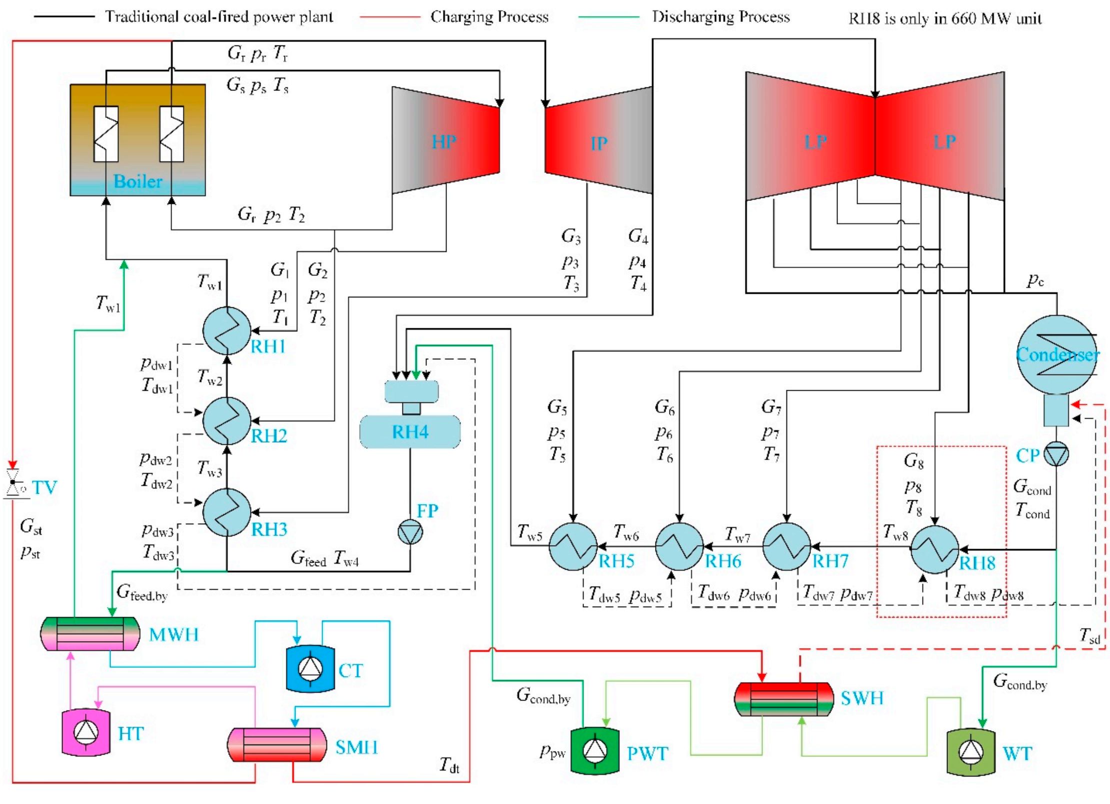

Figure 2. Flexible operation system of CFPU with reheated steam extraction and thermal energy storage.

In the load-reduction process, part of the reheated steam enters the IP and completes the thermal process of the system. Another part of the reheated steam is extracted and enters the SMH by iso-enthalpy depressurization in the throttle valve. The low-temperature molten salt from the CT is heated by the extracted reheated steam in SMH. The high-temperature molten salt flows into HT. The pressurized water is heated by the extracted reheated steam. The reheated steam extracted after cooling condenses into pressurized water, which then flows back to the condenser. The heated pressured water flows into the pressure water tank (PWT). Thus, the unit achieves the load-reduction operation.

The pressure water in PWT directly enters RH4, while the condensate water enters the water tank during the heat released process. The workflow of the feed water at the outlet of the feed water pump is the same as that in Figure 1.

2.3. Flexible Operation Mode

The designed parameters of 300 MW, 600 MW and 660 MW units in 100%THA are shown in Table 2.

Table 2. Design parameters of the unit at 100%THA.

State Point	Units	300 MW Unit	600 MW Unit	660 MW Unit	State Point	Units	300 MW Unit	600 MW Unit	660 MW Unit
Rated power	MW	300.19	600.18	660.02	p_4	MPa	0.76	1.02	1.20
p_s	MPa	16.67	16.67	26.47	T_4	°C	598.65	634.15	653.45
T_s	°C	811.15	811.15	873.15	p_5	MPa	0.53	0.62	0.48
G_s	t/h	958	1848.80	1878.90	T_5	°C	557.15	575.65	537.25
p_r	MPa	3.35	3.41	5.78	p_6	MPa	0.23	0.24	0.25
T_r	°C	811.15	811.15	893.15	T6	°C	464.40	469.45	470.95
G_r	t/h	790.35	1576.13	1599.15	p_7	kPa	79.90	81	110
p_1	MPa	5.80	6.08	8.08	T_7	°C	366.65	366.88	394.65
T_1	°C	656.35	658.45	680.35	p_8	kPa	/	/	40
p_2	MPa	3.73	3.79	6.29	T_8	°C	/	/	349.15
T_2	°C	598.05	595.65	645.25	p_c	kPa	15	15	11
p_3	MPa	1. 70	2.05	3.07	G_c	t/h	600.20	1218.29	1079.13
T_3	°C	707.85	734.65	792.95	G_{cond}	t/h	751.55	1457.65	1395.83

When investigating the flexible operation characteristics of the 300 MW, 600 MW and 660 MW units, the following assumptions should be made:

(1) The shaft seal leakage and valve stem leakage of the turbine should be ignored.
(2) The molten salts and phase-change materials are considered as ideal materials [21], which can meet the temperature requirements of each state points during the charging and discharging process.
(3) The pressure loss in the system is not considered.

Table 3 shows the flexible operation modes and its parameters of the 300 MW, 600 MW and 660 MW units.

Table 3. The mode of CFPU.

Flexible Operation Mode		Parameters in the Charging Process	Parameters in the Discharging Process
Cycle-I	Main steam extraction in 300 MW unit	$p_{st} = p_{dt} = p_{sd} = 1$ MPa $T_{dt} = 473.15$ K $T_{sd} = 448.15$ K	p_1, p_4, p_5, T_1, T_4 and T_5 is variable. $T_{cond} = 327.12$ K
Cycle-II	Main steam extraction in 600 MW unit	$p_{st} = p_{dt} = p_{sd} = 1$ MPa $T_{dt} = 473.15$ K $T_{sd} = 448.15$ K	p_1, p_4, p_5, T_1, T_4 and T_5 is variable. $T_{cond} = 327.12$ K
Cycle-III	Main steam extraction in 660 MW unit	$p_{st} = p_{dt} = p_{sd} = 1$ MPa $T_{dt} = 473.15$ K $T_{sd} = 448.15$ K	p_1, p_4, p_5, T_1, T_4 and T_5 is variable. $T_{cond} = 320.83$ K
Cycle-IV	Reheated steam extraction in 300 MW unit	$p_{st} = p_{dt} = p_{sd} = 0.5$ MPa $T_{dt} = 473.15$ K, $T_{sd} = 332.72$ K	p_1, p_4, T_1 and T_4 is variable. $T_{pw} = 393.36$ K, $T_{cond} = 327.12$ K
Cycle-V	Reheated steam extraction in 600 MW unit	$p_{st} = p_{dt} = p_{sd} = 0.5$ MPa $T_{dt} = 473.15$ K, $T_{sd} = 332.72$ K	p_1, p_4, T_1 and T_4 is variable. $T_{pw} = 393.36$ K, $T_{cond} = 327.12$ K
Cycle-VI	Reheated steam extraction in 660 MW unit	$p_{st} = p_{dt} = p_{sd} = 0.5$ MPa $T_{dt} = 473.15$ K, $T_{sd} = 326.43$ K	p_1, p_4, T_1 and T_4 is variable. $T_{pw} = 393.36$ K, $T_{cond} = 320.83$ K

3. Methodology and Validation

The system in this paper is explored using the first law of thermodynamics.

3.1. Charging and Discharging Process

During the loading process, the sensible/latent heat of the extraction is stored separately. The sensible/latent heat charging power is calculated based on Equations (1a,b) and (2), respectively. The total heat charging power is calculated based on Equation (3).

$$Q_{\mathrm{cha,Se}} = G_{\mathrm{st}}(h_{\mathrm{s}} - h_{\mathrm{dt}}) \tag{1a}$$

$$Q_{\mathrm{cha,Se}} = G_{\mathrm{st}}(h_{\mathrm{r}} - h_{\mathrm{dt}}) \tag{1b}$$

$$Q_{\mathrm{cha,La}} = G_{\mathrm{st}}(h_{\mathrm{dt}} - h_{\mathrm{sd}}) \tag{2}$$

$$Q_{\mathrm{cha}} = Q_{\mathrm{cha,Se}} + Q_{\mathrm{cha,La}} \tag{3}$$

The discharge power of the stored sensible heating bypass water and the stored latent heating bypass condensate water are calculated by Equations (4) and (5a,b). The total heat discharging power is calculated based on Equation (6).

$$Q_{\mathrm{discha,Se}} = G_{\mathrm{feed,by}}(h_{\mathrm{w1}} - h_{\mathrm{w4}}) \tag{4}$$

$$Q_{\mathrm{discha,La}} = G_{\mathrm{cond,by}}(h_{\mathrm{w5}} - h_{\mathrm{cond}}) \tag{5a}$$

$$Q_{\mathrm{discha,La}} = G_{\mathrm{cond,by}}(h_{\mathrm{pw}} - h_{\mathrm{cond}}) \tag{5b}$$

$$Q_{\mathrm{discha}} = Q_{\mathrm{discha,Se}} + Q_{\mathrm{discha,La}} \tag{6}$$

In order to ensure that the charging and discharging time of the sensible/latent heat is equal, the ratio of sensible heat power to the latent heat is defined by Equation (7).

$$\theta = \frac{Q_{\mathrm{cha,Se}}}{Q_{\mathrm{cha,La}}} = \frac{Q_{\mathrm{discha,Se}}}{Q_{\mathrm{discha,La}}} \tag{7}$$

$$Q_{\mathrm{cha}}\tau_{\mathrm{cha}}\eta^2\varepsilon = Q_{\mathrm{discha}}\tau_{\mathrm{discha}} \tag{8}$$

where η = 0.98 is the efficiency of the heat exchanger, and ε = 0.95 is the heat preservation coefficient.

3.2. Off-Design of Turbine

In the load-reduction process, the steam flow rate is reduced through the main steam extraction or the reheated steam extraction. In the load-raising process, the steam flow rate is increased through reducing the extracted steam flow rate of each extraction port of the turbine. So, the pressure at all stages is changed. Additionally, the off-design model can be calculated, as shown in Equation (9) [26].

$$\frac{G_{\mathrm{sTi}}}{G_{\mathrm{sT0i}}} = \sqrt{\frac{p_{\mathrm{sTi}}^2 - p_{\mathrm{sTi+1}}^2}{p_{\mathrm{sT0i}}^2 - p_{\mathrm{sT0i+1}}^2}}\sqrt{\frac{T_{\mathrm{sTi}}}{T_{\mathrm{sT0i}}}} \tag{9}$$

In the 300 MW unit and the 600 MW unit, $i = 1, 2, \cdots, 7$. In the 660 MW unit, $i = 1, 2, \cdots, 8$.

3.3. Flexible Operation Heat Balance of CFPU

The heat balance equation of the system is rebuilt by Equations (1)–(6) and (9), which is then shown in Equation (10). Equation (10a,b) are used in the main steam extraction scheme and the reheated steam extraction scheme, respectively.

$$\begin{bmatrix} q_1 & & & & & & & \\ \gamma_2 & q_2 & & & & & & \\ \gamma_3 & \gamma_3 & q_3 & & & & & \\ \gamma_4 & \gamma_4 & \gamma_4 & q_4 & & & & \\ & & & & q_5 & & & \\ & & & & \gamma_6 & q_6 & & \\ & & & & \gamma_7 & \gamma_7 & q_7 & \\ & & & & \gamma_8 & \gamma_8 & \gamma_8 & q_8 \end{bmatrix} \begin{bmatrix} G_1 \\ G_2 \\ G_3 \\ G_4 \\ G_5 \\ G_6 \\ G_7 \\ G_8 \end{bmatrix} + \begin{bmatrix} \\ \\ \\ G_{st}(h_{sd} - h_{w4}) \\ \\ \\ \\ \\ \end{bmatrix} = \begin{bmatrix} (G_{feed} - G_{feed,by})\varphi_1 \\ (G_{feed} - G_{feed,by})\varphi_2 \\ (G_{feed} - G_{feed,by})\varphi_3 \\ G_{cond}\varphi_4 \\ (G_{cond} - G_{cond,by})\varphi_5 \\ (G_{cond} - G_{cond,by})\varphi_6 \\ (G_{cond} - G_{cond,by})\varphi_7 \\ (G_{cond} - G_{cond,by})\varphi_8 \end{bmatrix} \tag{10a}$$

$$\begin{bmatrix} q_1 & & & & & & & \\ \gamma_2 & q_2 & & & & & & \\ \gamma_3 & \gamma_3 & q_3 & & & & & \\ \gamma_4 & \gamma_4 & \gamma_4 & q_4 & & & & \\ & & & & q_5 & & & \\ & & & & \gamma_6 & q_6 & & \\ & & & & \gamma_7 & \gamma_7 & q_7 & \\ & & & & \gamma_8 & \gamma_8 & \gamma_8 & q_8 \end{bmatrix} \begin{bmatrix} G_1 \\ G_2 \\ G_3 \\ G_4 \\ G_5 \\ G_6 \\ G_7 \\ G_8 \end{bmatrix} = \begin{bmatrix} (G_{feed} - G_{feed,by})\varphi_1 \\ (G_{feed} - G_{feed,by})\varphi_2 \\ (G_{feed} - G_{feed,by})\varphi_3 \\ (G_{cond} - G_{cond,by})\varphi_4 + G_{cond,by}(h_4 - h_{pw}) \\ (G_{cond} - G_{cond,by})\varphi_5 \\ (G_{cond} - G_{cond,by})\varphi_6 \\ (G_{cond} - G_{cond,by})\varphi_7 \\ (G_{cond} - G_{cond,by})\varphi_8 \end{bmatrix} \tag{10b}$$

where q_j, γ_j and φ_j are calculated by Equations (11)–(13) [27].

$$q_j = h_j - h_{dj} \tag{11}$$

$$\gamma_j = h_{dj-1} - h_{dj} \tag{12}$$

$$\varphi_j = h_{wj} - h_{wj+1} \tag{13}$$

In the 300 MW unit and 600 MW unit, $j = 1, 2, \cdots, 7$. In the 660 MW unit, $j = 1, 2, \cdots, 8$.

In the traditional CFPU, $G_{feed,by}$, $G_{cond,by}$ and G_{st} are 0.

In the charging process, $G_{feed,by}$ and $G_{cond,by}$ are 0, whereas G_{st} is variable.

In the discharging process, G_{st} is 0, $G_{feed,by}$ and $G_{cond,by}$ are variables, where $(h_4 - h_{pw})$ is variable.

3.4. Power Output

The power output of the CFPU is calculated in Equation (14).

$$\begin{aligned} W_T = {} & G_s(h_s - h_1) + (G_s - G_1)(h_1 - h_2) + (G_s - G_1 - G_2)(h_r - h_3) \\ & + \textstyle\sum_{m=3}^{k-1} \left((G_s - \sum_{j=1}^{m} G_j)(h_m - h_{m+1})\right) + (G_s - \sum_{j=1}^{k} G_j)(h_k - h_c) \end{aligned} \tag{14}$$

where k = 8 in the 660 MW unit, and k = 7 in the 300 MW unit and the 600 MW unit.

3.5. Boiler

The boiler and the turbine are running in the off-design in the charging and discharging process. The mass flow rate of the feed water and reheated steam is changed. The heat balance of the boiler should be recalculated by Equation (15).

$$G_{coal} LHV \eta_b = G_s(h_s - h_{w1}) + G_r(h_r - h_2) \tag{15}$$

where LHV = 29,270 kJ/kg, and η_b = 93.36%.

3.6. Thermal Efficiency

The thermal efficiency is an important indicator to evaluate the thermal economy of the CFPU, and can be calculated by Equations (16) and (17).

$$\eta_{thermal} = \frac{W_T}{G_{coal} LHV} \times 100\% \tag{16}$$

$$\eta_{\text{thermal}} = \frac{W_{\text{cha.T}}\tau_{\text{cha}} + W_{\text{discha.T}}\tau_{\text{discha}}}{(G_{\text{cha.coal}}\tau_{\text{cha}} + G_{\text{discha.coal}}\tau_{\text{discha}})LHV} \times 100\% \tag{17}$$

where η_{thermal} is the thermal efficiency of the CFPU, %.

3.7. Calculation Process

Figure 3 shows the calculation process for the operation system.

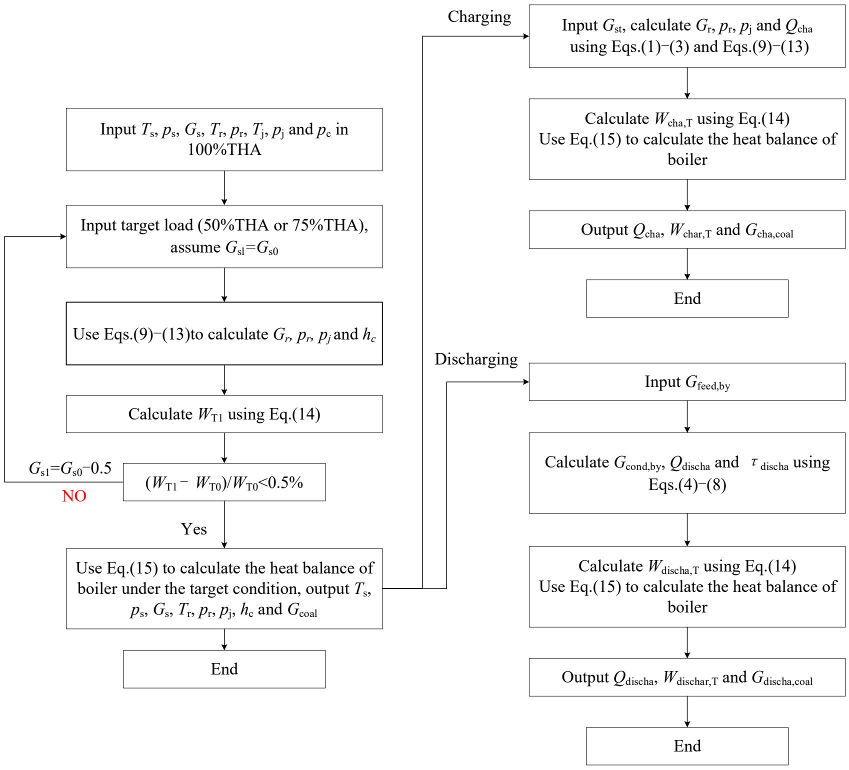

Figure 3. The calculation process for the operation system.

3.8. Errors Analysis

The errors between the designed value and the simulation value of 300 MW, 600 MW and 660 MW units in 100%THA are shown as Figure 3, the results of which are shown in Table 4. The error analysis results in this section are referenced in the literature by Wei et al. [21]. The maximum error among the three units is the exhaust steam flow of the 300 MW units, which is −2.28%. The reason for this error is that the shaft seal leakage is ignored, and the exhaust enthalpy is calculated by extrapolation curve. The error can meet the requirements of engineering accuracy [28].

Table 4. Error analysis.

		W_T (MW)	p_s (MPa)	G_s (t/h)	G_r (t/h)	G_{cond} (t/h)	G_c (t/h)
300 MW unit	Designed value	300.19	16.67	957.997	790.35	751.55	600.20
	Simulation value	300.19	16.67	945.92	801.40	737.18	586.50
	Error (%)	0	0	−1.26	1.40	−1.91	−2.28
600 MW unit	Designed value	600.18	16.67	1848.80	1576.13	1457.65	1218.29
	Calculated value	600.18	16.67	1843.59	1579	1443.60	1203.20
	Error (%)	0	0	−0.28	0.18	−0.96	−1.24
660 MW unit	Designed value	660.02	26.47	1878.90	1599.15	1395.83	1079.13
	Calculated value	660.00	26.47	1874.80	1603.80	1380.30	1059.70
	Error (%)	0	0	−0.22	0.29	−1.11	−1.8

4. Results and Discussion

4.1. Effect on the Unit Load and Charging Power in the Load-Reduction Process

Figure 4 shows the flow rate of extracted steam and the relationship of the 300 MW, 600 MW and 660 MW units under 50%THA in the load-reduction process. The steam flow into the turbine decreases with the increasing extracted steam flow rate. Due in part to the fact that the main steam does not enter the HP for working in the load-reduction process, the load-reduction capacity of the main steam extraction scheme is higher than that of the reheated steam extraction scheme. When the extracted steam flow rate of Cycle-I, Cycle-II, Cycle-III, Cycle-IV, Cycle-V and Cycle-VI is 90 t/h, 236.75 t/h, 223.50 t/h, 142 t/h, 290.50 t/h and 158.30 t/h, respectively, the unit load can be reduced to 38.64%THA, 34.48%THA, 35.23%THA, 34.37%THA, 33.95%THA and 40.59%THA, respectively.

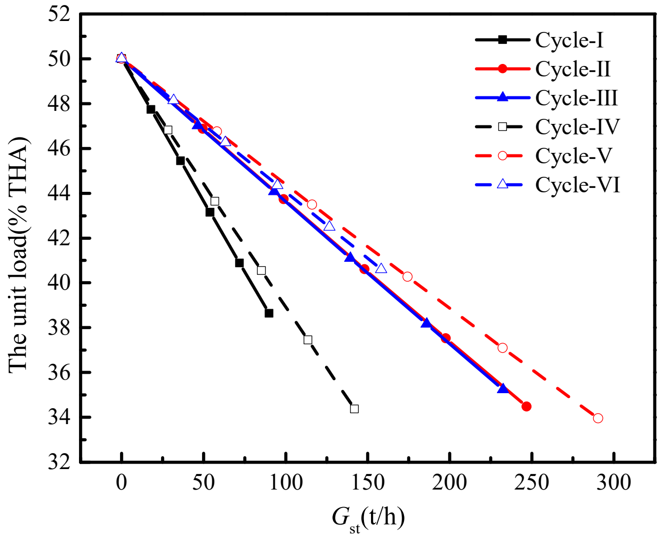

Figure 4. The trend of flow rate of extracted steam and unit load of 300 MW, 600 MW and 660 MW units under 50%THA in the load-reduction process.

Among the six load-reduction schemes, the load-reduction capacity presents different limit values. The heat released from the drainage water of RH3 and the extracted main steam to RH4 can meet the heat balance demand of RH4. When the extracted main steam flow rate increases, the heat balance of RH4 will be destroyed, which results in the generation of wet steam. It does not meet the safe operation of RH4. In Cycle-II, Cycle-IV and Cycle-V, the main factor limiting the load-reduction capacity is the steam flow rate into LP.

The blade of the last stage will generate negative work or vibrate when the steam flow rate at the inlet LP is lower than 30% of the rated steam flow rate of the LP, which affects the economy and safety of the unit. If the extracted steam flow rate continues to increase, RH8 needs to be cut off when the saturated temperature corresponds to the extracted steam port pressure of RH8 as the drainage temperature, which changes the operation mode of the original unit.

Figure 5 presents the trend of flow rate of extracted steam and unit load of the 300 MW, 600 MW and 660 MW units under 50%THA in the load-reduction process. The charging power is increased from 0 to 68.24 MW, 187.52 MW, 177.49 MW, 130.38 MW, 266.71 MW and 154.20 MW when the extracted steam flow rate of Cycle-I, Cycle-II, Cycle-III, Cycle-IV, Cycle-V and Cycle-VI during the load-reduction process is 90 t/h, 236.75 t/h, 223.50 t/h, 142 t/h, 290.50 t/h and 158.30 t/h, respectively. The charging powers of Cycle-I and Cycle-II are approximately equal at the same extracted main steam flow rate, which is caused by the approximately same temperature and pressure of the 300 MW and 600 MW units. The reason for this is that the charging powers of Cycle-IV and Cycle-V are approximately equal at the same extracted reheated steam flow rate. The charging power of Cycle-III is higher than that of Cycle-I and Cycle-II, and the charging power of Cycle-VI is higher than that of Cycle-IV and Cycle-V. The reason is that the temperature and pressure of the ultra-supercritical unit are higher than those of the subcritical unit. The charging power of the reheated steam extraction scheme is higher than that of the main steam extraction scheme. The reason for this is that the bigger steam pressure results in the lower enthalpy at the same steam temperature.

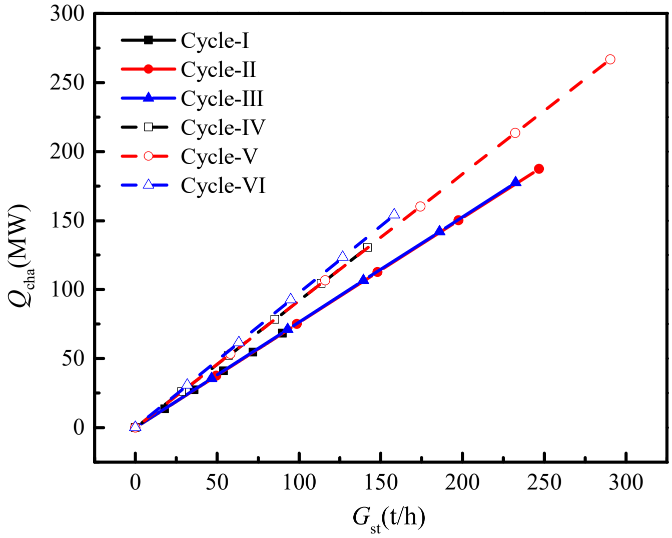

Figure 5. Relationship between extracted steam flow rate and charging power of 300 MW, 600 MW and 660 MW units under 50%THA in the load-reduction process.

4.2. Effect on Unit Load and Discharging Power in the Load-Raising Process

The stored heat is released to the original unit to increase the unit load in the load-raising process. Figure 6 shows the changes in discharging power of 300 MW, 600 MW and 660 MW with the bypassed condensate water flow rate and units under 50%THA in the load-raising process. The maximum bypassed condensate water flow rate can reach up to 396 t/h, 778 t/h, 724 t/h, 388.12 t/h, 753.59 t/h and 713.01 t/h of Cycle-I, Cycle-II, Cycle-III, Cycle-IV, Cycle-V and Cycle-VI, respectively; furthermore, the discharging power is 44.48 MW, 93.92 MW, 89.38 MW, 38.10 MW, 73.97 MW and 80.45 MW, respectively.

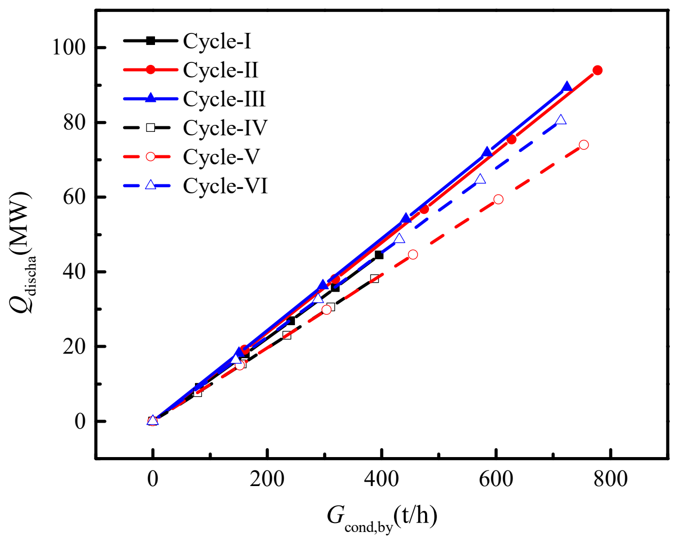

Figure 6. The changes in discharging power of 300 MW, 600 MW and 660 MW units with the bypassed condensate water flow rate and under 50%THA in the load-raising process.

The discharging power of the main steam extraction scheme is greater than that of the reheated steam extraction scheme at the same bypassed condensate water flow rate. Table 5 shows the ratio of the sensible/latent heat charging power. Since the temperature and pressure of the main/reheated steam of the ultra-supercritical unit are higher than those of the subcritical unit, the ratio of the ultra-supercritical unit is bigger than that of the subcritical unit. So, the discharging power is greater than that of the subcritical unit.

Table 5. Ratio of the sensible heat charging power to the latent heat charging power.

Work Mode	Cycle-I	Cycle-II	Cycle-III	Cycle-IV	Cycle-V	Cycle-VI
θ	0.3078	0.3095	0.3698	0.2684	0.2683	0.3322

Figure 7 shows the relationship between the discharging power and the unit load of the 300 MW, 600 MW and 660 MW units under 50%THA in the load-raising process. The raising discharging power increases the unit load. The unit load of Cycle-I, Cycle-II, Cycle-III, Cycle-IV, Cycle-V and Cycle-VI is increased to 53.77%THA, 54.16%THA, 53.81%THA, 53.07%THA, 53.01%THA and 53.28%THA when the discharging power is 44.48 MW, 93.92 MW, 89.38 MW, 38.10 MW, 73.97 MW and 80.45 MW, respectively, which is increased by 3.77%, 4.16%, 3.81%, 3.07%, 3.01% and 3.28% compared with the unit load of 50%THA. For the same reason as in Figure 6, the unit load increment of the main steam extraction scheme is greater than that of the reheated steam extraction scheme. The load increment of the 300 MW unit is greater than that of the 600 MW and 660 MW units at the same discharging power. The reason is that the flow rate of main steam of 300 MW unit is about half of 600 MW and 660 MW units. The impact of the same discharging power (or bypassed condensate water flow) on the steam pressure of each stage of the 300 MW unit is much greater than that of the 600 MW and 660 MW units, which results in a larger load increment of the 300 MW unit.

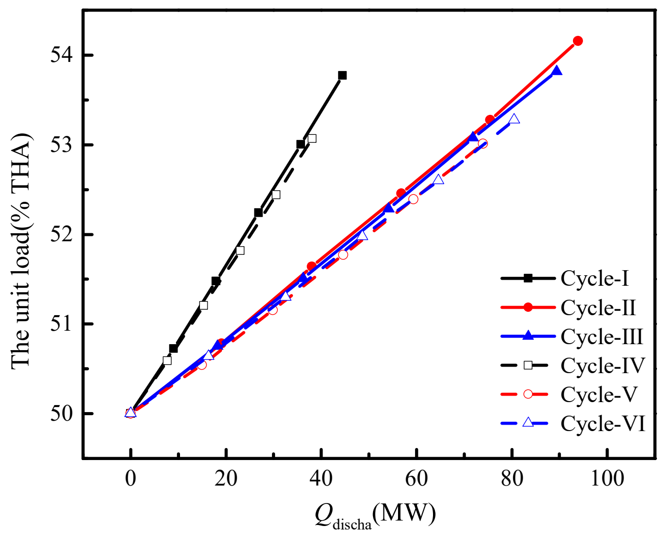

Figure 7. Relationship between discharging power and unit load of 300 MW, 600 MW and 660 MW units under 50%THA in the load-raising process.

Figure 8 shows the changes in discharging power of the 300 MW, 600 MW and 660 MW units with the bypassed condensate water flow rate under 75%THA in the load-raising process. The changing relationship is similar to that in Figure 6. Due to the rising unit load, the main steam flow rate is increasing. The maximum flow rate of the bypassed condensate water in Cycle-I, Cycle-II, Cycle-III, Cycle-IV, Cycle-V and Cycle-VI is 602.50 t/h, 1165.50 t/h, 1093.50 t/h, 570.31 t/h, 1091.90 t/h and 1042.60 t/h, and the discharging power is 81.47 MW, 167.01 MW, 159.25 MW, 55.98 MW, 107.17 MW and 117.64 MW, respectively.

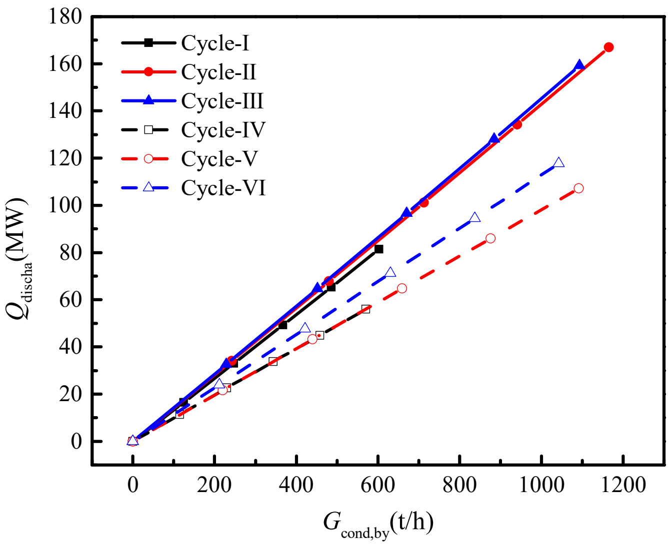

Figure 8. Relationship between bypassed condensate water flow rate and discharging power of 300 MW, 600 MW and 660 MW units under 75%THA in the load-raising process.

Figure 9 shows the relationship between the discharging power and the unit load of the 300 MW, 600 MW and 660 MW units under 75%THA in the load-raising process. The changing relationship is similar to that in Figure 7. When the discharging power of Cycle-I, Cycle-II, Cycle-III, Cycle-IV, Cycle-V and Cycle-VI is 81.47 MW, 167.01 MW, 159.25 MW, 55.98 MW, 107.17 MW and 117.64 MW, respectively, in the load-raising process, the unit load is increased to 82.54%THA, 83.01%THA, 82.34%THA, 79.60%THA, 79.40%THA and 79.87%THA, respectively, which is increased by 7.54%, 8.01%, 7.34%, 4.60%, 4.40% and 4.87%, respectively, compared with the unit load of 75%THA.

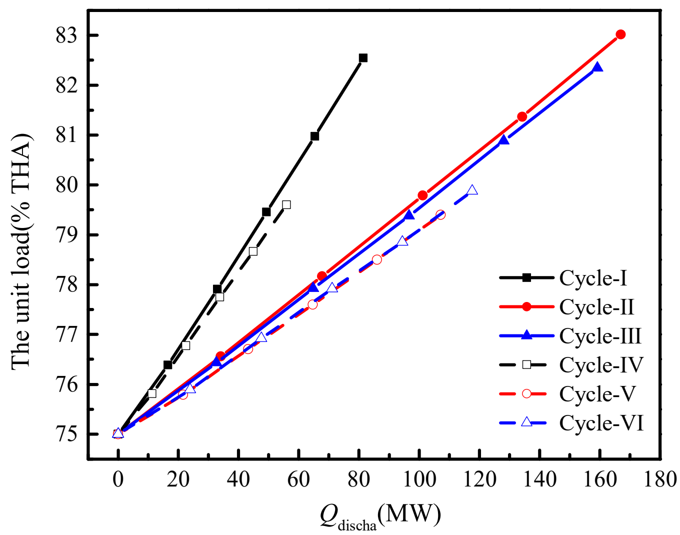

Figure 9. Relationship between discharging power and unit load of 300 MW, 600 MW and 660 MW units under 75%THA in the load-raising process.

The unit load increment of 75%THA is greater than that of 50%THA at the same discharging power. The reason is that the steam pressure of the turbine under 75%THA is higher than that of under 50%THA. The higher steam pressure has the greater work capacity; thus, the load increment of 75%THA is larger. Due to the maximum discharging power under 75%THA being greater than that under 50%THA, the maximum load increment of the unit under 75%THA is higher than that of the unit under 50%THA. The impact of the main steam extraction scheme on the maximum load increment is greater than that of the reheated steam extraction scheme. The reason is that the latent heat stored by the phase-change materials can heat the bypassed condensate water to the outlet temperature of RH5 under any working condition in the discharging process. When using the pressured water to store the latent heat, the pressure is a constant value, and the pressured water does not participate in temperature regulation. The pressure water with lower temperature results in the larger extracted steam flow rate of RH4. So, the load increment in the reheated steam extraction scheme is not obvious.

According to Figures 4, 7 and 9, the load operation range of the unit can be achieved when the unit is running at the load-reduction mode under 50%THA, at the load-raising mode under 50%THA, and at the load-raising mode under 75%THA, as shown in Figure 10. When the unit completes the load-reduction and load-raising operation under 50%THA, the unit load operation ranges of Cycle-I, Cycle-II, Cycle-III, Cycle-IV, Cycle-V and Cycle-VI are 38.64–53.77%THA, 34.48–54.16%THA, 35.23–53.81%THA, 34.37–53.07%THA, 33.95–53.01% THA and 40.59–53.28%THA, respectively. When the unit completes the load-reduction operation under 50%THA and load-raising operation under 75%THA, the unit load-operation ranges of Cycle-I, Cycle-II, Cycle-III, Cycle-IV, Cycle-V and Cycle-VI are 38.64–82.54% THA, 34.48–83.01%THA, 35.23–82.34%THA, 34.37–79.60%THA, 33.95–79.40%THA and 40.59–79.87%THA, respectively. The results show that the unit load operation range of Cycle-II is the largest from the perspective of flexible operation load regulation. The scheme of Cycle-II is the best, and Cycle-III is second.

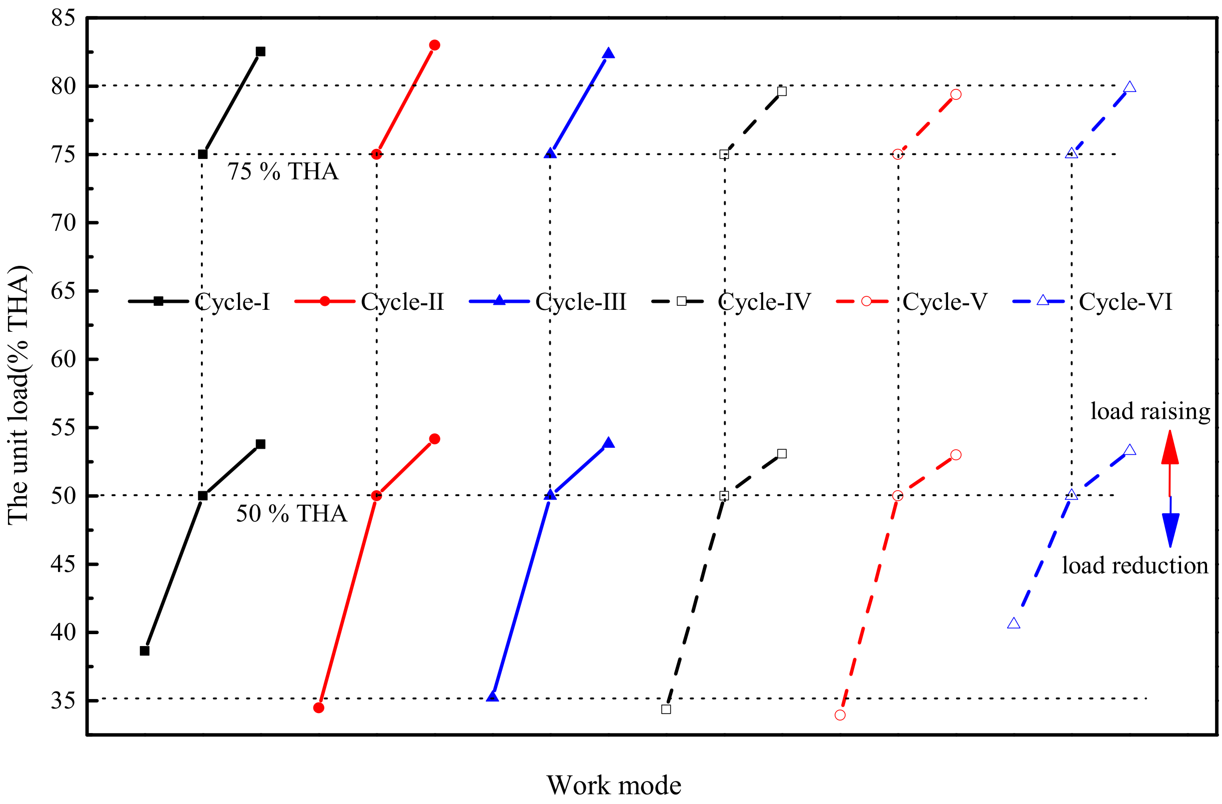

Figure 10. Unit load operation range.

4.3. Effect on Charging and Discharging Time

The ratio of the discharging time is achieved under condition of load-reduction operation under 50%THA and load-raising operation under 50%THA, and under the condition of load-reduction operation under 50%THA and load-raising operation under 75%THA, respectively, as shown in Figures 11 and 12.

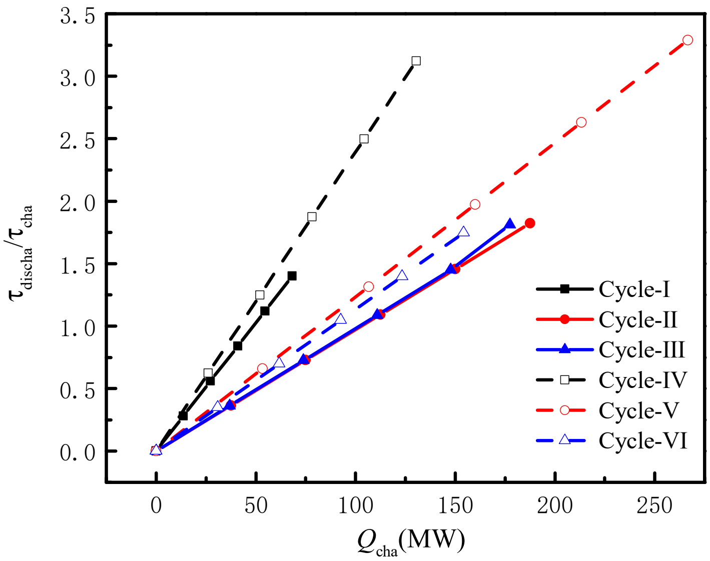

Figure 11. The ratio of discharging time to charging time under the conditions of a load-reduction operation under 50%THA and a load-raising operation under 50%THA.

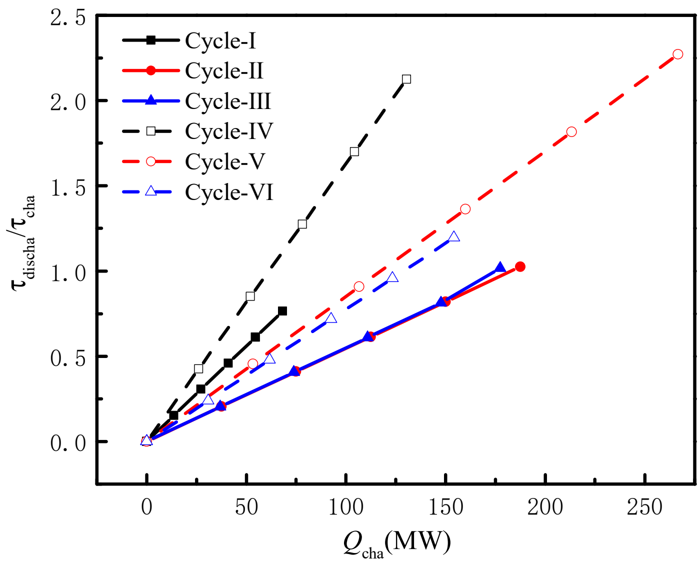

Figure 12. The ratio of discharging time to charging time under the conditions of a load-reduction operation under 50%THA and a load-raising operation under 75%THA.

When the unit completes the load-reduction and load-raising operation under 50%THA, the maximum ratio of the discharging time to the charging time of Cycle-I, Cycle-II, Cycle-III, Cycle-IV, Cycle-V and Cycle-VI is 1.40, 1.82, 1.81, 3.12, 3.29 and 1.75, respectively, which reveals that the unit can complete peak shaving operation for 10 h/day, 8.51 h/day, 8.54 h/day, 5.81 h/day, 5.59 h/day and 8.73 h/day. When the unit completes the load-reduction operation under 50%THA and load-raising operation under 75%THA, the maximum ratio of the discharging time to the charging time of Cycle-I, Cycle-II, Cycle-III, Cycle-IV, Cycle-V and Cycle-VI is 0.76, 1.02, 1.02, 2.12, 2.27 and 1.20, respectively, which indicates that the unit can complete peak shaving operation for 13.64 h/day, 11.88 h/day, 11.88 h/day, 7.69 h/day, 7.34 h/day and 10.91 h/day. The ratio of the discharging time to the charging time and the peak shaving time are shown in Table 6. The results show that Cycle-I has the longest peak shaving time for the flexible operation. However, the load operation range of Cycle-I is lower than that of Cycle-II and Cycle-III. Cycle-II and Cycle-III are better in terms for flexible operation range and the peak shaving time.

Table 6. Ratio of discharging time to charging time and peak shaving time.

	Cycle-I	Cycle-II	Cycle-III	Cycle-IV	Cycle-V	Cycle-VI
Load-reduction operation and load-raising operation under 50%THA						
Ratio of discharging time to charging time	1.40	1.82	1.81	3.13	3.29	1.75
Peak shaving time	10	8.51	8.54	5.81	5.59	8.73
Load-reduction operation under 50%THA and load-raising operation under 75%THA						
Ratio of discharging time to charging time	0.76	1.02	1.02	2.12	2.27	1.20
Peak shaving time	13.64	11.88	11.88	7.69	7.34	10.91

4.4. Effect on Thermal Efficiency

The thermal efficiency of the unit is obtained by taking the calculation conditions and the calculation data described in Section 4.3. The thermal efficiency difference between the thermal efficiency of base load and the thermal efficiency of flexible operation can be calculated by Equation (18). The difference in thermal efficiency is shown in Figures 13 and 14.

$$\Delta\eta_{\text{thermal}} = \eta_{\text{thermal}} - \eta_{\text{base}} \tag{18}$$

where $\Delta\eta_{\text{thermal}}$ is the thermal efficiency difference, %, and η_{base} is the thermal efficiency at base load, %.

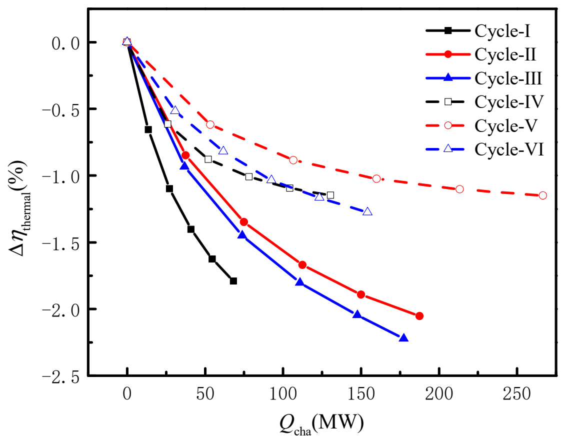

Figure 13. The thermal efficiency difference under the conditions of a load-reduction operation under 50%THA and a load-raising operation under 50%THA.

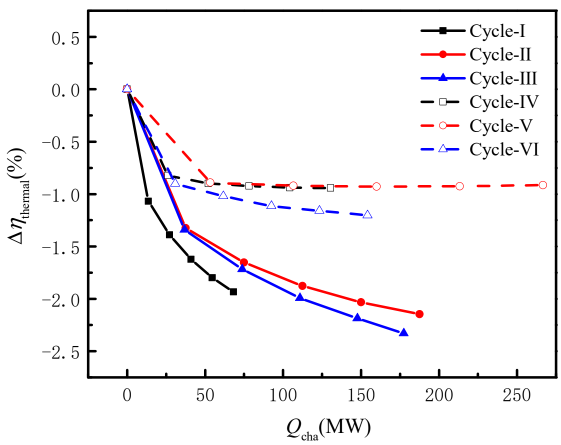

Figure 14. The thermal efficiency difference under the conditions of a load-reduction operation under 50%THA and a load-raising operation under 75%THA.

The thermal efficiency difference of the unit rises with the increase in the charging power (extracted steam flow rate). The thermal efficiency difference increases with the rising charging power. When the unit completes the load-reduction and load-raising operation under 50%THA, the thermal efficiency of Cycle-I, Cycle-II, Cycle-III, Cycle-IV, Cycle-V and Cycle-VI is decreased by 1.79%, 2.05%, 1.81%, 1.15%, 1.15% and 1.28%, respectively. When the unit completes the load-reduction operation under 50%THA and load-raising operation under 75%THA, the thermal efficiency of Cycle-I, Cycle-II, Cycle-III, Cycle-IV, Cycle-V and Cycle-VI is decreased by 1.93%, 2.15%, 2.33%, 0.94%, 0.92% and 1.20%, respectively.

The thermal efficiency difference sequence of the three units Is the 600 MW unit, 660 MW unit and 300 MW unit in the scheme of main steam extraction and reheated steam extraction at the same charging power. The reason is that the 660 MW unit is the ultra-supercritical unit, and the pressure loss is greater than that of 600 MW unit in steam extraction process; thus, its thermal efficiency decreases more. On the one hand, the number of blade stages of the 660 MW unit low-pressure cylinder is less than that of the 600 MW unit, and the blade length of the 660 MW unit low-pressure cylinder is higher than that of the 600 MW unit low-pressure cylinder. On the other hand, the initial parameter of the 660 MW unit is higher than that of the 600 MW unit, and when the load reduction is the same (e.g., 10% THA), the efficiency of the low-pressure cylinder of the 660 MW unit is lower than that of the low-pressure cylinder of the 600 MW unit. Therefore, the thermal efficiency of the 660 MW unit decreases more than the 600 MW unit. Additionally, the thermal performance of 300 MW unit is lower than that of 600 MW and 660 MW units; thus, its thermal efficiency is the lowest. The results indicate that the scheme of reheated steam extraction is the best for flexible operation from the perspective of thermal efficiency. The reheated steam extraction scheme is more suitable for the 600 MW unit.

5. Conclusions

In order to achieve a synergistic relationship between the steam extraction parameters and thermal parameters of different types of coal-fired power units, this paper investigates the influence of thermal parameters of the 300 MW subcritical unit, the 600 MW subcritical unit and the 660 MW ultra-supercritical unit on the thermal adaptability of flexible operation. The following conclusions are drawn.

(1) The load regulation range of the 300 MW, 600 MW and 660 MW units under six operation modes is different. The maximum load-reduction capacity can be achieved by adopting the scheme the reheated steam extraction in the 600 MW unit; moreover, the load can be reduced to 33.95%THA from 50%THA.

(2) The main steam extraction scheme is suitable for the wide load flexibility regulation in the regard of load range and peak shaving time. The load range of the main steam extraction scheme of the 600 MW unit is the largest. When the unit completes a load-reduction and load-raising operation under 50%THA, the load range is 34.48–54.16%THA, and the peak shaving time is 8.51 h/day. When the unit completes a load-reduction operation under 50%THA and load-raising operation under 75%THA, the load range is 34.48–83.01%THA, and the peak shaving time is 11.88 h/day.

(3) The scheme of reheated steam extraction is ideal for low load flexibility regulation from the perspective of thermal efficiency. When the 600 MW unit with the reheated steam extraction scheme completes a load-reduction and load-raising operation under 50%THA, the thermal efficiency is reduced by only 1.15%.

Although this article conducted thermal adaptability analysis on 300 MW, 600 MW, and 660 MW units, the investment and economic feasibility of their retrofitting were not analyzed. In subsequent work, the author will discuss investment costs and optimization plans, carbon emission patterns during peak shaving and the coupling scheduling relationship between peak shaving and renewable energy sources. The method used will adjust the optimal ratio of renewable energy and coal-fired units in the power grid, and can better guide the promotion of carbon peaking and carbon neutrality.

Author Contributions: Investigation Writing—original draft H.W.; Formal analysis Methodology—review & editing Y.L.; Writing review & editing Y.Y.; Validation Writing Y.W.; Resources Conceptualization K.Z.; Project administration Supervision L.L. All authors have read and agreed to the published version of the manuscript.

Funding: This research received no external funding.

Data Availability Statement: The data used to support the findings of this study are available from the corresponding author upon request.

Conflicts of Interest: Author Liang Li was employed by the company Inner Mongolia Daihai Power Generation Co., Ltd. The remaining authors declare that the research was conducted in the absence of any commercial or financial relationships that could be construed as a potential conflict of interest.

Nomenclature

Abbreviations	
CFPU	coal-fired power unit
THA	turbine heat acceptance
RH	regenerative heat exchanger
HP	high-pressure steam turbine
IP	intermediate-pressure steam turbine
LP	low-pressure steam turbine
SMH	steam–molten salt heat exchanger
MWH	molten salt–water heat exchanger
SWH	steam–water heat exchanger
PCH	phase-change heat exchanger
PWT	pressured water tank
WT	water tank
CT	cold molten salt tank
HT	hot molten salt tank
Symbols	
Q	heat power, MW
G	mass flow rate, t/h
T	thermodynamic temperature, K
p	pressure, MPa
h	specific enthalpy, kJ/kg
LHV	lower heating value of coal, kJ/kg
W	power output of the unit, MW
q	enthalpy difference of steam, kJ/kg
Greek	
τ	time, h
γ	enthalpy difference of drainage water, kJ/kg
φ	enthalpy difference of water, kJ/kg
θ	ratio of sensible heat power to the latent heat power
Subscripts	
T	turbine
sT	stage of turbine
dw	drainage water
w	water
feed	feed water
feed,by	bypassed feed water
cond	condensate water
cond,by	bypassed condensate water
coal	coal feeding into boiler
s	main steam
r	reheat steam
c	exhaust steam of low-pressure steam turbine
sd	drainage water of extracted steam
cha	charging process

discha	discharging process
dt	dividing temperature
0	parameters before off-design
Se	sensible heat of extracted steam
La	latent heat of extracted steam

References

1. Wang, Z.; Diao, Y.; Zhao, Y.; Chen, C.; Liang, L.; Wang, T. Thermal performance of integrated collector storage solar air heater with evacuated tube and lap joint-type flat micro-heat pipe arrays. *Appl. Energy* **2020**, *261*, 114466. [CrossRef]
2. Ding, Z.; Wu, W. A hybrid compression-assisted absorption thermal battery with high energy storage density/efficiency and low charging temperature. *Appl. Energy* **2021**, *282*, 116068. [CrossRef]
3. Wang, C.; Song, J.; Zhu, L.; Zheng, W.; Liu, Z.; Lin, C. Peak shaving and heat supply flexibility of thermal power plants. *Appl. Therm. Eng.* **2021**, *193*, 117030. [CrossRef]
4. Gomaa, M.R.; Mustafa, R.J.; Al-Dmour, N. Solar thermochemical conversion of carbonaceous materials into syngas by Co-Gasification. *J. Clean. Prod.* **2020**, *248*, 119185. [CrossRef]
5. Wang, C.; Liu, M.; Li, B.; Liu, Y.; Yan, J. Thermodynamic analysis on transient cycling of coal-fired power plants: Simulation study of a 660 MW supercritical unit. *Energy* **2017**, *122*, 505–527. [CrossRef]
6. Zhang, L.; Cui, J.; Zhang, Y.; Yang, T.; Li, J.; Gao, W. Performance analysis of a compressed air energy storage system integrated into a coal-fired power plant. *Energy Convers. Manag.* **2020**, *225*, 113446. [CrossRef]
7. Hasan, N.S.; Hassan, M.Y.; Majid, S.; Rahman, H.A. Review of storage schemes for wind energy systems. *Renew. Sustain. Energy Rev.* **2013**, *21*, 237–247. [CrossRef]
8. Hou, H.; Xu, T.; Wu, X.; Wang, H.; Tang, A.; Chen, Y. Optimal capacity configuration of the wind-photovoltaic-storage hybrid power system based on gravity energy storage system. *Appl. Energy* **2020**, *271*, 115052. [CrossRef]
9. Alptekin, E.; Ezan, M.A. Performance investigations on a sensible heat thermal energy storage tank with a solar collector under variable climatic conditions. *Appl. Therm. Eng.* **2020**, *164*, 114423. [CrossRef]
10. Xu, B.; Chen, D.; Venkateshkumar, M.; Xiao, Y.; Yue, Y.; Xing, Y.; Li, P. Modeling a pumped storage hydropower integrated to a hybrid power system with solar-wind power and its stability analysis. *Appl. Energy* **2019**, *248*, 446–462. [CrossRef]
11. Zhao, Y.; Wang, C.; Liu, M.; Chong, D.; Yan, J. Improving operational flexibility by regulating extraction steam of high pressure heaters on a 660MW supercritical coal-fired power plant: A dynamic simulation. *Appl. Energy* **2018**, *212*, 1295–1309. [CrossRef]
12. Wang, J.; Huo, J.; Zhang, S.; Teng, Y.; Li, L.; Han, T. Flexibility Transformation Decision-Making Evaluation of Coal-Fired Thermal Power Units Deep Peak Shaving in China. *Sustainability* **2021**, *13*, 1882. [CrossRef]
13. Lebedev, V.; Deev, A. Heat Storage as a Way to Increase Energy Efficiency and Flexibility of NPP in Isolated Power System. *Appl. Sci.* **2023**, *13*, 13130. [CrossRef]
14. Wei, H.; Lu, Y.; Yang, Y.; Zhang, C.; Wu, Y.; Li, W.; Zhao, D. Flexible Operation Mode of Coal-fired Power Unit Coupling with Heat Storage of Extracted Reheat Steam. *J. Therm. Sci.* **2022**, *31*, 436–447. [CrossRef]
15. Cao, R.; Zhang, Z.; Zhao, C.; Han, C.; Bao, W.; Yu, D. A novel thermal power unit with feedwater pump turbine driven by thermal energy storage system: System construction and performance evaluation. *Int. J. Energy Res.* **2022**, *46*, 19438–19450. [CrossRef]
16. Zhang, H.; Liang, W.; Liu, J.; Wang, J. Modeling and Energy Efficiency Analysis of Thermal Power Plant with High Temperature Thermal Energy Storage (HTTES). *J. Therm. Sci.* **2020**, *29*, 1025–1035. [CrossRef]
17. Chen, C.; Ge, Z.; Zhang, Y. Study of combined heat and power plant integration with thermal energy storage for operational flexibility. *Appl. Therm. Eng.* **2023**, *219*, 119537. [CrossRef]
18. Liu, X.; Zhang, L.; Jin, K.; Xue, X.; Zhou, H. Integration model and performance analysis of coupled thermal energy storage and ejector flexibility retrofit for 600 MW thermal power units. *J. Clean. Prod.* **2023**, *428*, 139337. [CrossRef]
19. Cao, R.; Lu, Y.; Yu, D.; Guo, Y.; Bao, W.; Zhang, Z.; Yang, C. A novel approach to improving load flexibility of coal-fired power plant by integrating high temperature thermal energy storage through additional thermodynamic cycle. *Appl. Therm. Eng.* **2020**, *173*, 115225. [CrossRef]
20. Fu, Y.; Ning, Z.; Ge, W.; Fan, Q.; Zhou, G.; Ma, T. Using Molten-Salt Energy Storage to Decrease the Minimum Operation Load of the Coal-Fired Power Plant. *Therm. Sci.* **2020**, *24*, 2757–2771. [CrossRef]
21. Wei, H.; Lu, Y.; Yang, Y.; Zhang, C.; He, C.; Wu, Y.; Li, W.; Zhao, D. Research on influence of steam extraction parameters and operation load on operational flexibility of coal-fired power plant. *Appl. Therm. Eng.* **2021**, *195*, 117226. [CrossRef]
22. Wang, B.; Ma, H.; Ren, S.; Si, F. Effects of integration mode of the molten salt heat storage system and its hot storage temperature on the flexibility of a subcritical coal-fired power plant. *J. Energy Storage* **2023**, *58*, 106410. [CrossRef]
23. Ma, T.; Li, Z.; Lv, K.; Chang, D.; Hu, W.; Zou, Y. Design and performance analysis of deep peak shaving scheme for thermal power units based on high-temperature molten salt heat storage system. *Energy* **2024**, *288*, 129557. [CrossRef]
24. Cao, L.; Li, Y.; Si, H. Research on Temperature Distribution Characteristics in Low Pressure Cylinder of Large Steam Turbine Under Ultra-low Load Conditions. *Proc. Chin. Soc. Electr. Eng.* **2021**, *41*, 1018–1025.
25. Cao, L.; Xu, M.; Luo, H.; Si, H. Strain-life estimation of the last stage blade in steam turbine during low volume flow conditions. *Eng. Fail. Anal.* **2021**, *125*, 105399. [CrossRef]

26. Zhai, R.; Liu, H.; Li, C.; Zhao, M.; Yang, Y. Analysis of a solar-aided coal-fired power generation system based on thermo-economic structural theory. *Energy* **2016**, *102*, 375–387. [CrossRef]
27. Wu, J.; Hou, H.; Hu, E.; Yang, Y. Performance improvement of coal-fired power generation system integrating solar to preheat feed water and reheated steam. *Sol. Energy* **2018**, *163*, 461–470. [CrossRef]
28. Liu, H.; Zhai, R.; Patchigolla, K.; Turner, P.; Yang, Y. Off-design thermodynamic performances of a combined solar tower and parabolic trough aided coal-fired power unit. *Appl. Therm. Eng.* **2021**, *183*, 116199. [CrossRef]